

Research Article

Investigating Supercritical Bended Flow Using Physical Model and CFD

Hamza Souli , Jihane Ahattab , and Ali Agoumi 

Hassania School of Public Works, Casablanca, Morocco

Correspondence should be addressed to Hamza Souli; souli.hamza.cedoc@ehp.ac.ma

Received 1 December 2022; Revised 12 February 2023; Accepted 20 February 2023; Published 16 March 2023

Academic Editor: Houari Ameur

Copyright © 2023 Hamza Souli et al. This is an open access article distributed under the Creative Commons Attribution License, which permits unrestricted use, distribution, and reproduction in any medium, provided the original work is properly cited.

The flow in the bend channel used as spillway chute is complex due to the turbulence, the presence of shock waves, and vibrations. These transverse waves can damage the hydraulic structure. Our aim in this paper is to investigate the distribution of water surface in five curved channels with five relative curvatures p , different bottom slopes (1%, 2%, 10%, and 18%) and three different cross-sections. The objective is to give a solution to reduce the height difference between the inner and the outer walls. To achieve this goal, we used physical models to investigate the flow patterns, explore critical zones, and test several solutions to have a better performance. The reliability and accuracy of the numerical results were validated using the physical modelling for each case tested. Moreover, a comparison between the measured data, theoretical calculations, and numerical outcomes was done, to find a fitting law between the maximum wave height and the bend number. Furthermore, an optimal position of the guide wall was identified in real project of a spillway. The results of the physical model and numerical simulation show a good agreement; thus, the numerical model can play a crucial role in order to study hydraulic parameters, pressure, and velocity field and find solutions for hydraulic problems that occur in these structures.

1. Introduction

It is well known that topographical and geological conditions make it sometimes inevitable to construct spillways with bends. These bends in spillway chute play a major role in creating perturbations, shock waves [1], and vibrations. This can lead to serious hydraulic problems like cavitation in the chute of spillways and after the gates of the bottom outlet [13–14].

In the aim to understand the behaviour of these transverse waves called also rooster tail waves [2–4] for supercritical flows in the bend chute, a plethora of studies were done by several authors.

Ippen and Knapp [5] presented the first study. They conducted several tests with different relative radii of curvature, and they gave the first formula in order to estimate the maximum and minimum of the wave height that occurs in the bend channel.

Reinauer and Hager [6–9] studied the supercritical bend flow using experimentations. They described the flow in

these conditions and the wave extrema as a function of the bend number and wave profiles with the help of three channels.

Some other researchers who focused on the same topic were introduced by [10–12] using 2D shallow water equations in order to compute the hydraulic parameters of the bend flow.

In the literature, we found two types of bend flow:

- (i) Weak bend flow: The profile of water between the outer and inner wall is almost trapezoidal and continuous.
- (ii) Strong bend flow: The flow is separated, and we observe high water levels in the outer wall in comparison with the inner wall. Also, the transverse surface profile almost has the shape of a triangle [13, 14].

Furthermore, the bend supercritical flow creates shock waves; thus, the flow breaks into high unstable hydraulic jumps with huge amount of air entrainment, and this results

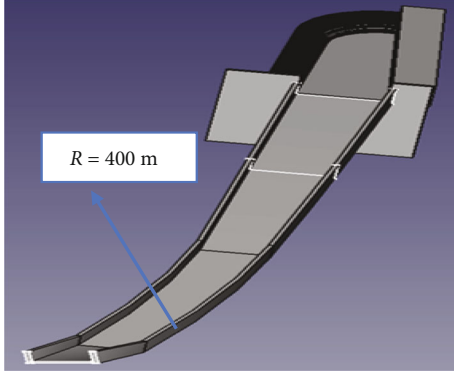


FIGURE 1: Side channel spillway with curved chute $R = 400$ m.

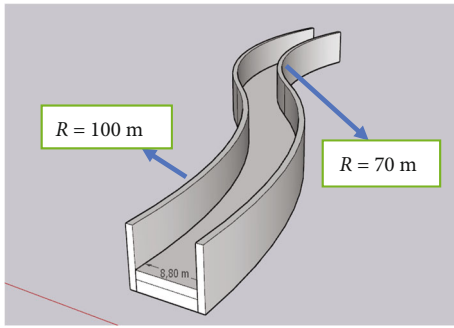


FIGURE 2: Bottom outlet with two curvatures $R = 70$ m and $R = 100$ m.

in significant hydraulic problems, namely cavitation, that can damage the chutes [15–18].

Moreover, the height of these rooster tail waves increases with the increase of the Froude number and the amount of aeration on the flow [19], [1].

The goal of this research is to simulate case studies:

- (i) Three curved channels with different ρ .
- (ii) Bottom outlet with two curvatures downstream the gates.
- (iii) Curved spillway chute.

The aim is to comprehend the flow behaviour, the effect of slope, and relative curvature $\rho = b/R$ for different head discharges ($H = 1 - 4$ m). And compare it with numerical modelling using Flow 3D Hydro in terms of the hydraulic parameters such as the water surface, velocity field, and Froude number. The second objective is to validate the solution of the separating wall. The dividing wall plays a crucial role for balancing the water profile and avoiding the creation of a vortex or a zone of stagnation of flow by the formation of a hydraulic jump. The zone of stagnation, which is created for the low head discharges, generates a problem of detachment of the jet in the ski jump, because the flow does not have enough kinetic energy to take off further away from the dam.

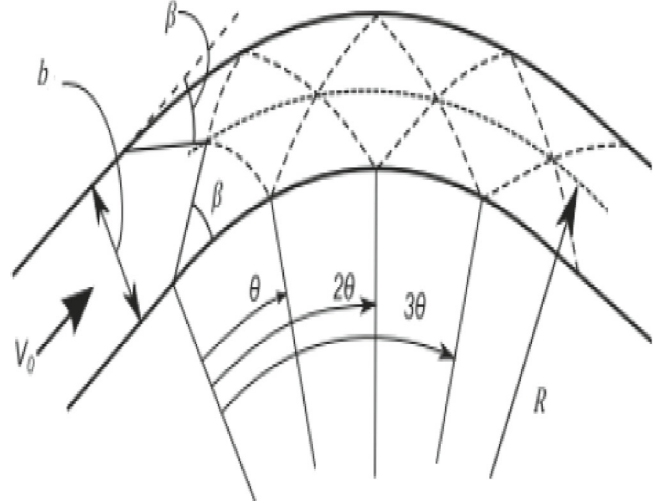


FIGURE 3: The model of shock waves in a curvature of a rectangular channel in supercritical regime [13].

Five physical models were used in order to investigate the flow behaviour, patterns, velocity field, and maximum height in the curvature and to validate these results.

2. Materials and Methods

2.1. Physical Model. The experiments are completely based on a 3D physical model for this study in order to observe the effect of 3D conditions, and to have a better idea about the flow behaviour.

The experimental facility is composed of:

- (i) The upstream part is a rectangular basin with dimensions (10 m \times 20 m).
- (ii) The downstream part is also a rectangular basin in order to study the problem in relation with scour issues; this part is beyond the scope of this article.

Instrumentation



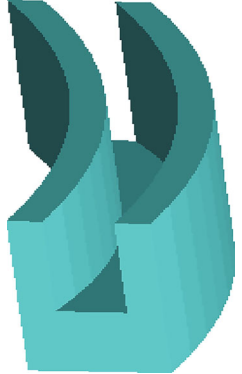
- (i) Rolling point instrumentation with high accuracy is used to measure the flow height above the weir (± 1 mm).
- (ii) Dynamic pressure sensor with frequency 500 Hz ($\pm 0.05\%$).
- (iii) Magnetic flow meter to measure the flow rate ($\pm 0.5\%$).
- (iv) Pitot tube to measure the velocity ($\pm 0.1\%$).

Physical model of the spillway is based on the Froude similitude defined by:

$$F_r = \frac{V}{\sqrt{gh}}. \quad (1)$$

To ensure that we have similar flows between model and prototype with less scale effect, we must verify certain

TABLE 1: Curved channels tested by CFD and theoretical calculations.

Geometry			
Curvature R (m)	70 m	40 m	50 m
Width B (m)	8.8 m	3 m	2 m
Relative curvature ρ	0.125	0.075	0.04
Bottom slope	1% 2%	10%	10%
Length (m)	37 m	20 m	26 m

criteria that depend on two numbers Re (Reynolds number) and We (Weber number), defined by the following equations:

$$Re = \frac{Vh}{\nu}, \quad (2)$$

$$We = \frac{\rho h V^2}{\sigma}. \quad (3)$$

We know that the air transport in the model is influenced essentially by scale effect; therefore, the following conditions must be verified:

- (i) $Re_{\text{model}} > 1$ to 2.5×10^5
- (ii) $We^{0.5} > 110$ to 170 [19]

The geometry of side channel spillway with a curved chute shown in Figure 1 for our case study is composed of:

- (i) Side channel trough with L-shaped weir.
- (ii) Curved channel with radius of curvature of 400 m.
- (iii) Ski jump at the end as an energy dissipator.

For the second case study, the curved shown in Figure 2 is composed of:

- (i) A channel with a width of 8.8 m and two radii of curvature of 100 m and 70 m.
- (ii) The length is 133 m and has a slope of 1%.
- (iii) Two walls on each side of the channel with a height of 5 m.

In order to examine and explore the flow patterns and to test the supercritical flow for bend channel, five models with a scale of 1/40 were used.

To understand the effect of curvature and bottom slope in the channels of hydraulic structures, we varied the relative curvature from 0.075 to 0.125, and the bottom slope from 1% to 18%.

We opted for the choice of testing several variants numerically and then validating the results using the experimental data.

In the first part, we will test several geometries (see Table 1) for different slopes and different ρ , to try to understand the behaviour of the collisions of the water surface with the walls of the curved channels, by theoretical calculations, numerical, and physical modelling.

We will give the maximum values of the water height for each case, the water surface for each wave angle θ varied from 0° to 30° .

For the curved spillway chute, the head discharges varied between 0.5 m and 4.8 m [8].

For the case study of the bottom outlet, we tested the head discharge $H = 5$ m.

Samples of the laboratory data will be given in comparison with the numerical approaches for each part of the present research.

We study, for the case of the bottom outlet, the part after the gates, the free surface part that is composed of two curvatures with two radii of curvatures 100 m and 70 m, respectively (Figure 2).

A calculation of the increase of the water level in this part is made in order to verify the passage of the design head discharge. The flow is supercritical, and so gravity waves manifest in the curvature.

A comparison between the water surfaces from the physical model with that of the computational fluid dynamics

TABLE 2: Mesh convergence analysis.

H (m)	ρ	Slope	Cell size (m)	Total number of cells
1 m, 2 m, 3 m, 4 m	0.125	1%–2%	0.5 m	81,584
			0.2 m	709,724
			0.1 m	3,009,825
1 m, 2 m, 3 m, 4 m	0.075	10%	0.2 m	300,000
1 m, 2 m, 3 m, 4 m	0.04	10%	0.2 m	215,000
4 m–5 m	0.0125–0.088	1%	0.2 m	3,000,259
0.5 m–4.8 m	0.09	18%	0.5 m	16,256,000
			0.7 m	5,000,276

TABLE 3: The constants of turbulence model.

σ_ε	$C_{1\varepsilon}$	$C_{2\varepsilon}$	σ_k	η_0	β	C_μ
0.71942	1.42	1.68	0.71942	4.38	0.012	0.0845

(CFD) is done, and the verification of the maximum and minimum depth of water surface in order to avoid overflow over the walls.

2.2. Theoretical Calculations. The change in the direction of flow generated in the curved channels, in supercritical regime, gives rise to two shock waves: a positive producing an increase in water depth and a negative involving a depth less than the uniform depth [6] (see Figure 3(a)).

Due to the transverse waves, Figure 3 shows the formation of shock waves in the walls in the form of zigzags (wave interference principle). It has been shown that these interferences are created in positions where they are the multiples of the wave angle θ , for example, 2θ , 3θ ... (see Figure 3).

The angle β formed by the two wave fronts with the initial direction of flow depends on the Froude number upstream of the curvature F_0 and is given approximately by the following equations:

$$\sin(\beta) = \frac{1}{F_0}. \quad (4)$$

The angle θ is determined, as a function of the width of the spillway chute b and the radius of the curve R , by:

$$\tan(\theta) = \frac{b/R}{(1 + b/2R) \tan(\beta)}. \quad (5)$$

The maximum and minimum water heights are estimated using the following formula:

$$h_{\min}^{\max} = h F_0^2 \sin^2\left(\beta \pm \frac{\theta}{2}\right), \quad (6)$$

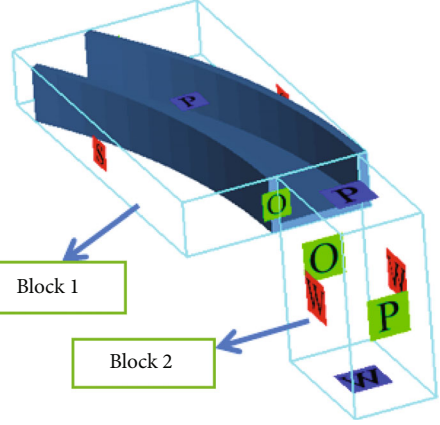


FIGURE 4: Implementation of the boundary conditions.

$$\begin{cases} \theta = \arctan\left(\frac{b/R}{(1 + b/2R) \tan(\beta)}\right) \\ \theta = \tan\left(\frac{b}{R} F_0\right) \text{ for high values of } F_0 \text{ with } \frac{b}{R} < \frac{1}{2} \end{cases} \quad (7)$$

The angle θ indicates the place where, along the curved channel, a maximum and a minimum of the height of water on the sidewalls are established for the first time.

2.3. Hydraulic Tests. Reinauer and Hager [6] carried out experimental work on the hydraulic characteristics of supercritical flow in a curved rectangular channel, whose objective is to define the velocity distribution and the flow area across the curve.

Concerning the velocity distribution, these tests show that the velocity remains constant across the channel and is equal to the approach velocity V_0 with the exception of the boundary layer and the wall separation zones.

As for the water surface, the torrential flow leads to significant variations across the channel. For small values of mean curvature $\rho_a = b/R_a$, the maximum heights (index e) along the inner and outer walls are given by:

$$Y_e = \frac{h_e}{h_0} = \left(1 \pm \frac{1}{2} \rho_a F_0^2\right)^2 = \left(1 \pm \frac{1}{2} B_0^2\right)^2. \quad (8)$$

This shows that the product in equation (7) is involved in this phenomenon, and that the Froude number dominates the structure of the shock waves.

From an experimental point of view, only the number B_0 , called the Bend number, must vary instead of an independent variation of the Froude number and the relative curvature.

In practice, we are mainly interested in the maximum heights of shock waves to size the walls. Let h_M be the maximum height along the curve and h_m be the corresponding

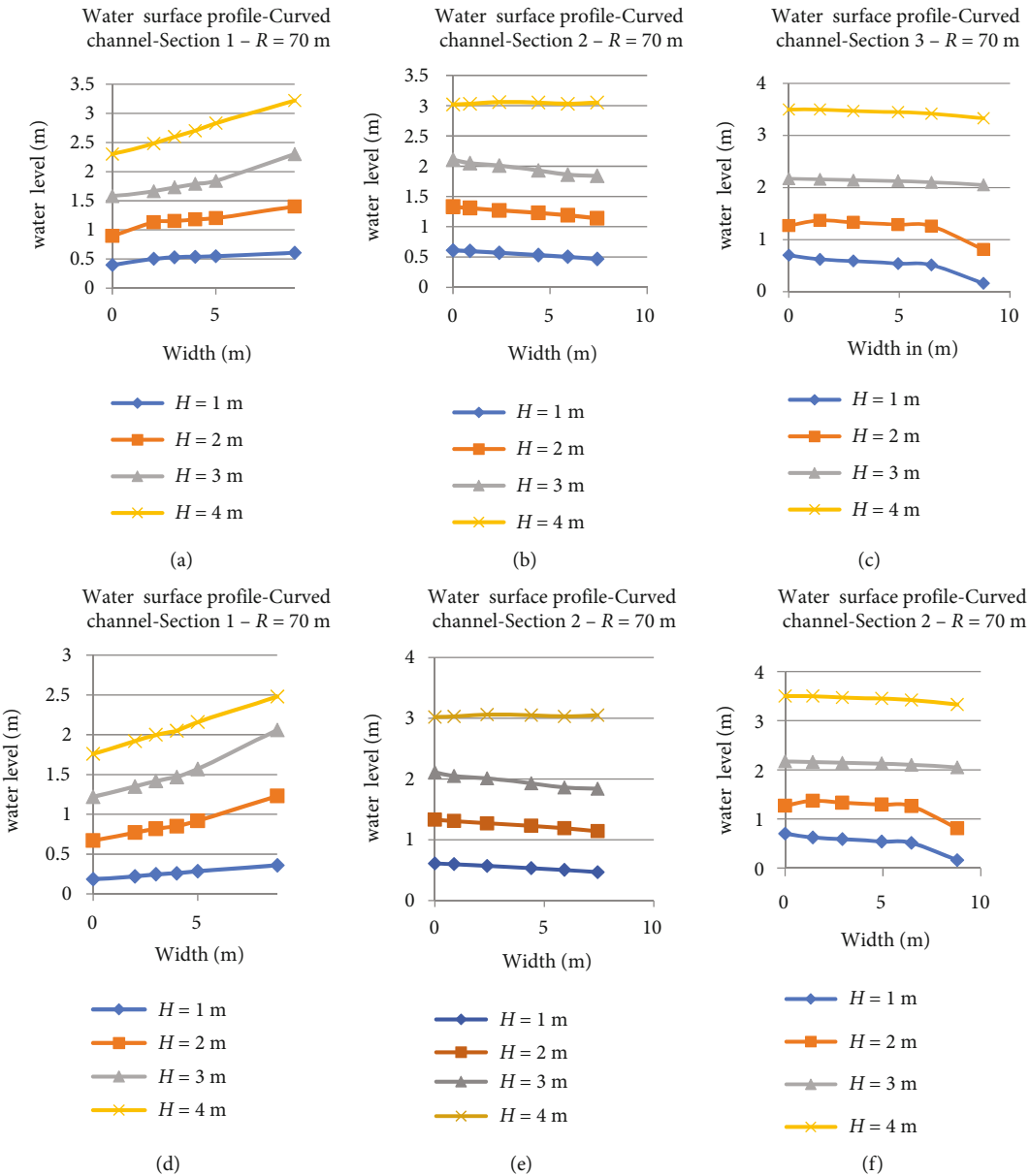


FIGURE 5: Continued.

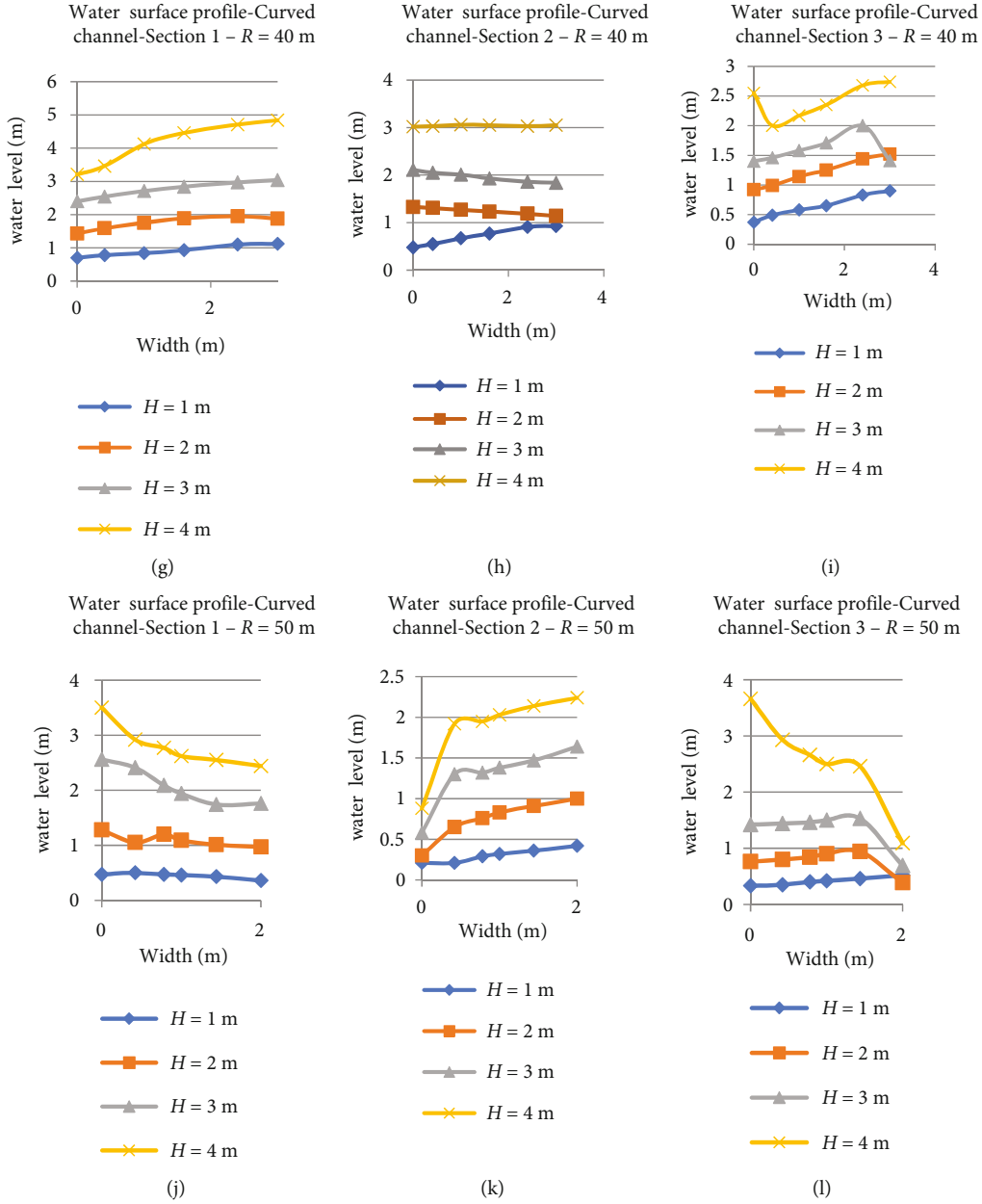


FIGURE 5: Cross-section water level for the tested cases.

minimum height. So $Y_M = h_M/h_0$ and $Y_m = h_m/h_0$ be the relative values. Hydraulic tests yielded the following results:

$$\begin{cases} Y_M = (1 + 0.4B_0^2)^2 & \text{For } B_0 \leq 1.5 \\ Y_M = (1 + 0.6B_0)^2 & \text{For } B_0 > 1.5 \end{cases} \quad (9)$$

The location of extreme waves defined by the angles, θ_M and θ_m , respectively depends on the product $\rho_a F_0$ and are as follow:

$$\begin{cases} \tan(\theta_M) = \rho_a F_0 & \text{For } \rho_a F_0 \leq 0.35 \\ \tan(\theta_M) = 0.6(\rho_a F_0)^{1/2} & \text{For } \rho_a F_0 > 0.35 \end{cases} \quad (10)$$

The minimum wave height is given by the exact relationship (giving Y_e):

$$\begin{cases} Y_m = (1 - 0.5B_0^2)^2 \\ \tan(\theta_m) = 2^{0.5} \rho_a F_0 \end{cases} \quad (11)$$

3. Numerical Model

There are many steps in order to build the numerical model [20–22]:

- (i) Definition of the objective of the modelling: this step is crucial for understanding our system and the initial parameters.

TABLE 4: Power law of the maximum wave height.

ρ	θ	Coefficients		R^2
		α	β	
0.125 slope = 1%	10°	0.0097	-6.61	0.97
	20°	0.267	-2.055	0.985
	30°	0.89	-0.951	0.985
0.125 slope = 2%	10°	0.244	-3.03	0.993
	20°	0.62	-1.609	0.86
	30°	0.61	-2.15	0.72
0.075	10°	1.71	-1.33	0.94
	20°	1.763	-1.268	0.94
0.04	10°	0.73	-2.54	0.99
	20°	1.54	-1.73	0.75

TABLE 5: Polynomial law of the maximum wave height.

ρ	θ	A	Coefficients		R^2
			B	C	
0.075	30°	7.75	-17.4	11.72	0.96
0.04	30°	5.17	-11.094	7.35	0.997

- (ii) Specification of the models in terms of the hypothesis, the scale of resolving the problem, and the flexibility of the model.
- (iii) Defining the mathematical model.
- (iv) Choosing the parameters that influence our system, sensitivity analysis, the modelling approach, and methods of resolution.
- (v) Methods of choosing the initial parameters (theoretical calculations, empirical data, benchmarking ...).
- (vi) Fixing the criteria in terms of convergence, stability, and accuracy in the aim to guarantee the performance of the model.
- (vii) Verifying the results and the outcomes of the system by testing and checking.
- (viii) Estimating the uncertainties that depend on the purposes of the model.

For the geometry, we use the Free CAD software [23] in order to draw the geometry of the case studies.

We used the software Flow 3D Hydro, which is the best CFD software, for free surface flows in the objective to model the flow for supercritical bend flow.

For the totality of the numerical simulations, the following models were used:

- (i) The order of accuracy is second order.
- (ii) Pressure solver: implicit.

(iii) Viscous stress solver: explicit and sometimes Successive Overrelaxation Method (SOR).

(iv) Momentum advection: second order.

(v) Fluid flow solver: solve momentum and continuity equations.

3.1. Grid Sensitivity Analysis. A grid convergence analysis involving different size of mesh was done for each case study in order to select the adequate proper cell size.

The grid convergence study shows that for curved channel with $\rho = 0.125, 0.075, 0.04, 0.088$, the optimal cell size is 0.2 m (see Table 2).

The correct value of the cell size is found by comparing the computed values of the hydraulic parameters with those found in the physical modelling.

For the whole side spillway with curved chute, we used two cell sizes of 0.5 m and 0.7 m, and we found that the proper cell size is 0.5 m.

The total number of meshes varies between 80,000 cells and 16 million.

Table 2 summarizes the tested cases with the size and number of cells for each case tested.

3.2. Turbulence Modelling: RANS Governing Equations. As in most engineering applications, we use RANS model (Reynolds-averaged Navier-Stokes equations) in order to model turbulence.

For our simulation, we utilize the RANS equations (RNG $k - \epsilon$), in order to close the system and obtain the algebraic equations using finite volume approach. Flow 3D computes the mean values for the hydraulic parameters for each cell using a staggered grid system [21].

The resolution of these governing (), with the help of the constants from Table 3, gives the velocity, pressure field, and the tracking of the water surface (equation (23)).

The governing equations and the constants used are as follow.

$$\frac{\partial k}{\partial t} + \frac{\partial k u_i}{\partial x_i} - \frac{\partial}{\partial x_i} \left(\mu_{k_{\text{eff}}} \frac{\partial k}{\partial x_i} \right) = G - \epsilon, \quad (12)$$

$$\frac{\partial \epsilon}{\partial t} + \frac{\partial \epsilon u_i}{\partial x_i} - \frac{\partial}{\partial x_i} \left(\mu_{\epsilon_{\text{eff}}} \frac{\partial \epsilon}{\partial x_i} \right) = (C_{1\epsilon} - R_\epsilon) \frac{\epsilon}{k} G - C_{2\epsilon} \frac{\epsilon^2}{k}, \quad (13)$$

$$D_{k_{\text{eff}}} = \nu_t + \nu, \quad (14)$$

$$\mu_{\omega_{\text{eff}}} = \alpha_{\omega t} \nu_t + \nu, \quad (15)$$

$$\mu_{\epsilon_{\text{eff}}} = \frac{\nu_t}{\sigma_\epsilon} + \nu, \quad (16)$$

$$\nu_t = C_\mu \frac{k^2}{\epsilon}, \quad (17)$$

$$S_{ij} = \frac{1}{2} \left(\frac{\partial u_j}{\partial x_i} + \frac{\partial u_i}{\partial x_j} \right), \quad (18)$$

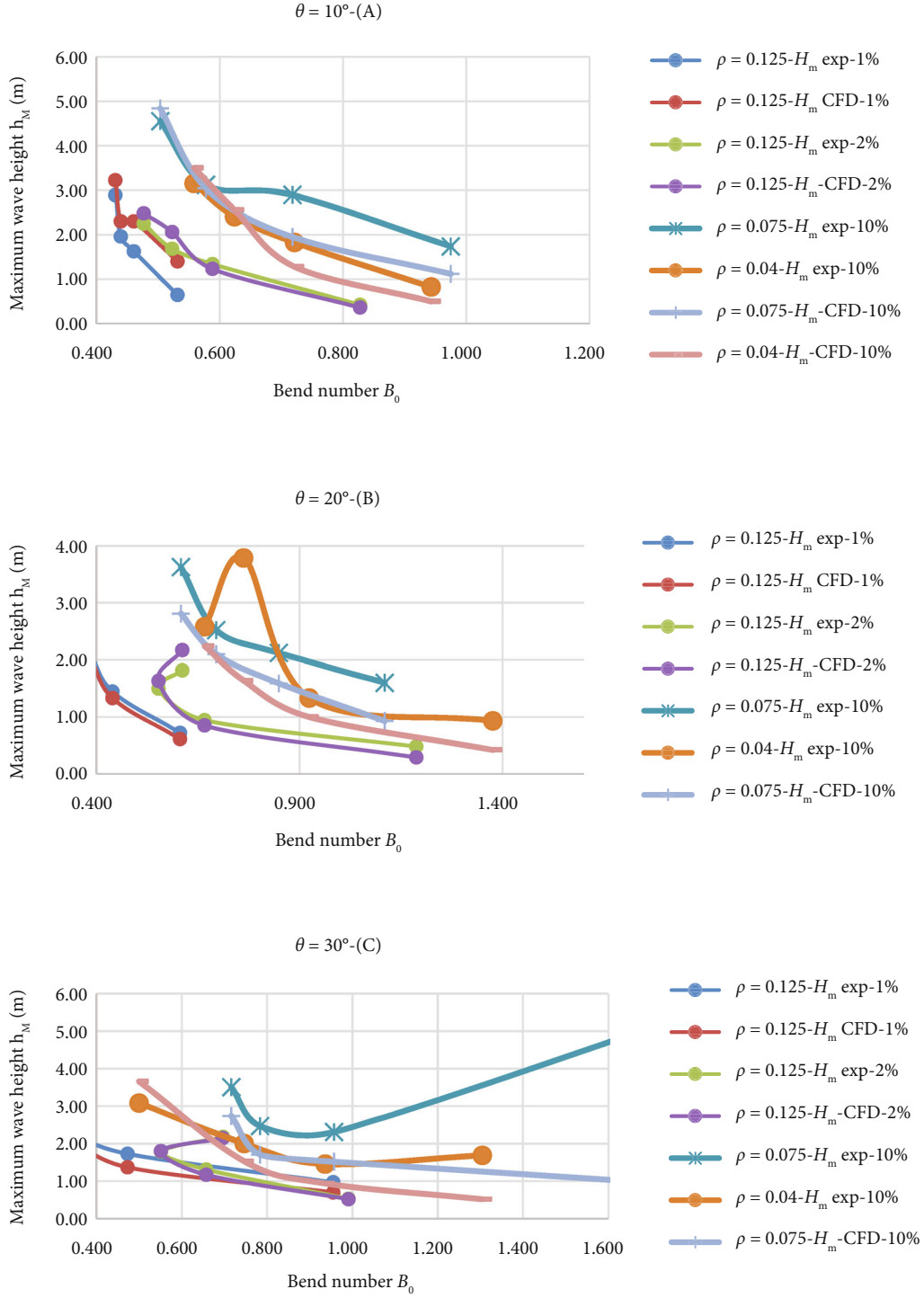


FIGURE 6: The maximum height as a function of the number for the three-tested section.

$$S_2 = 2S_{ij}S_{ij}, \quad (19)$$

$$\eta = \sqrt{S_2} \frac{k}{\varepsilon}. \quad (22)$$

$$G = 2\nu_t S_{ij}S_{ij}, \quad (20)$$

$$R_\varepsilon = \frac{\eta(1 - (\eta/\eta_0))}{1 + \beta^3}, \quad (21)$$

3.3. *Free Surface Modelling.* The volume of fluid (VOF) approach can estimate the water surface.

The VOF method utilizes the fraction function α as an indicator in order to determine the percentage of the cell full of water, air, or both[12].

TABLE 6: Water level for bottom outlet using theoretical calculations.

First curvature $R = 100$ m		
θ	H_{\max} (m)	H_{\min} (m)
0	1.45	—
$\theta = 18^\circ$	3.9	0.17
$2\theta = 36^\circ$	3	1.22
Second curvature $R = 70$ m		
θ	H_{\max} (m)	H_{\min} (m)
0	2.11	—
$\theta = 14^\circ$	3.34	1.11
$2\theta = 28^\circ$	3.4	1.26
$3\theta = 42^\circ$	4.3	1.39

The software utilizes the Tru-VOF method for tracking the interface between water and air.

The VOF equation for interface tracking is:

$$\frac{\partial \alpha}{\partial t} + u_i \frac{\partial \alpha}{\partial x_i} = 0. \quad (23)$$

3.4. *Boundary Conditions.* The four frequent boundary conditions are:

- (i) S (symmetry): This is the default condition indicating that you have no conditions to check on this facet or that you are working with a control volume.
- (ii) W (wall): Indicates that the facet is a wall containing the flow.
- (iii) P (specified pressure): Represents the pressure in meters that may correspond to the elevation of the fluid on a facet or the fraction of the fluid equal to 0 (total absence of water) to designate the atmosphere on the facet at the top of the mesh.
- (iv) O (outflow): Illustrates the facets that can discharge the outflow. To avoid water, build up in the block.

Figure 4 shows the boundary conditions used in the tested cases.

We have opted for the choice of two blocks in order to optimize the solution and the numerical calculation time.

For block 1: the inlet boundary was specified with a fixed pressure (head discharge), the bottom and sidewalls were set as no-slip condition with equivalent roughness $k_s = 0.015$ mm according to the Plexiglas surface properties. The top boundary is fixed as atmospheric pressure ($p = 0$). The outlet boundary was configured as outflow is set to zero-gradient condition in order to let the flow enter to the block 2.

For block 2: the inlet boundary was specified with outlet condition, the sidewalls were set as symmetry condition. The top boundary is fixed as atmospheric pressure ($p = 0$). The

TABLE 7: Right water level-physical model.

Distance (m)	Cumulative distance (m)	Water level (m)
0	0	1.39
12.94	12.94	1.62
14.17	27.11	2.76
13.77	40.88	4.39
13.75	54.63	4.35
13.32	67.95	3.51
15.06	83.01	2.45
12.56	95.57	1.14
13.71	109.28	0.56
14.75	124.03	0.11
9.01	133.04	0.93

outlet boundary was configured as outflow and is set to zero-gradient condition (see Figure 4).

4. Results and Discussion

4.1. *The Water Level in the Cross-Sections.* The simulated water surface profiles at three cross-sections for each case tested.

The water surface for each section is found for θ values 10° , 20° , and 30° , respectively.

We have chosen these positions because in these regions, the maximum height of the water surface is located.

For the relative curvature $\rho = 0.125$ with a slope of 1% and for a curved channel with a width of 8.8 m, for the three sections, the water level in the cross-section increases with the increase of the head discharges, and a maximum of the water height is observed at the right wall (see Figures 5(a), 5(b), and 5(c)).

In the first section, we observe that the water level increase sharply unlike the other Sections 2 and 3, the variation of the water surface is moderate.

For the relative curvature $\rho = 0.125$ with a slope of 2% and for a curved channel with a width of 8.8 m, for the three sections, the water level in the cross-section increases with the increase of the head discharges (see Figures 5(d), 5(e), and 5(f)).

Only small deviations can be found in comparison with the water surface with the same geometrical parameters.

The slope accelerates the flow but reduces the water level slightly.

The same flow patterns can be seen in section number 3. The minimum height is recorded in this section, because the flow has dissipated a portion of its hydraulic energy due to friction with the curved channel sidewalls.

For the relative curvature $\rho = 0.075$ with a slope of 10% and for a curved channel with a width of 3 m, for the three sections, the water level in the cross-section increases with the increase of the head discharges (see Figures 5(g), 5(h), and 5(i)).

The water level for the first section jumped rapidly with the increase of the head discharges.

For the second section, for head discharge $H = 1$ m, it can be noticed that the water profile rose up quickly in comparison with discharges higher than 1 m, the other water surfaces remain nearly steady.

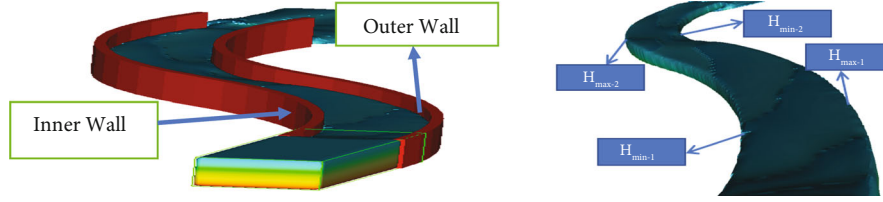


FIGURE 7: Numerical modeling of the bottom outlet-water surface.



FIGURE 8: Water surface and rooster tail waves for the bottom outlet in the physical model.

For Section 3, for $H < 2$ m, the water profile went up sharply, and reaches the maximum height. For head discharges $H > 2$ m, the water level shows some fluctuations; furthermore, the water surface is unstable for these charges due to the presence of shock waves and water wings.

For the relative curvature = 0.04 with a slope of 10% and for a curved channel with a width of 2 m, for the three sections, the water level in the cross-section increases with the increase of the head discharges (see Figures 5(j), 5(k), and 5(l)).

The water level for the first section dropped rapidly with the increase of the head discharges.

For the second section, for head discharge $H = 1$ m, it can be seen that the water profile maintains a constant level comparison with discharges higher than 1 m, the other water surfaces climbed steeply.

For section 3, for $H < 2$ m, the water profile remains slightly constant. For head discharges $H > 2$ m, the water level shows some fluctuations and water wings (rooster tail waves).

The novelty of these abacuses is that they allow an estimation of the wave height in these cross-sections for the aim of sizing the sidewalls for the initial design.

4.2. Fitting the Maximum Height in Curved Channels Using Power and Second Order Polynomial Laws. We have shown

that the maximum height in the studied sections of the curved channels follows a power law for more than 83% of the sections (10 sections out of 12), and the others follow a polynomial law as a function of the bend number B_0 .

It has been shown that the maximum wave height h_M follows two fitting laws for the case tested with correlation coefficient R^2 between 0.72 and 0.997 (see Tables 4 and 5).

The wave height is given by the empirical formula (equation (24)):

$$\left\{ h_M = \frac{\alpha B_0^\beta}{AB_0^2 + BB_0 + C} \right. \quad (24)$$

The novelty of these fitting laws is that we can estimate the maximum height h_M using Figures 6(a), 6(b), and 6(c), in order to estimate the height of the sidewalls in the curved channels, the local velocity at each section, the Froude number in the phase of initial design, and thereafter validate the optimal variant by the physical model with an optimization of the cost of construction of the physical models and also the computational cost.

The figures give a comparison between the values calculated by the numerical modelling noted CFD and values derived from the physical modelling noted exp.

These graphs allow obtaining the statistical fitting laws for the different tested cross-sections ($\theta = 10^\circ, 20^\circ, 30^\circ$).

TABLE 8: Left water level-physical model.

Distance (m)	Cumulative distance (m)	Water level (m)
0	0	1.66
12.37	12.37	1.63
13.05	25.42	0.78
12.29	37.71	0.57
13.53	51.24	0.27
13.9	65.14	0.68
11.39	76.53	2.22
14.24	90.77	3.32
12.98	103.75	4.48
11.54	115.29	4.71
13.16	128.45	3.59
4.6	133.05	3.65

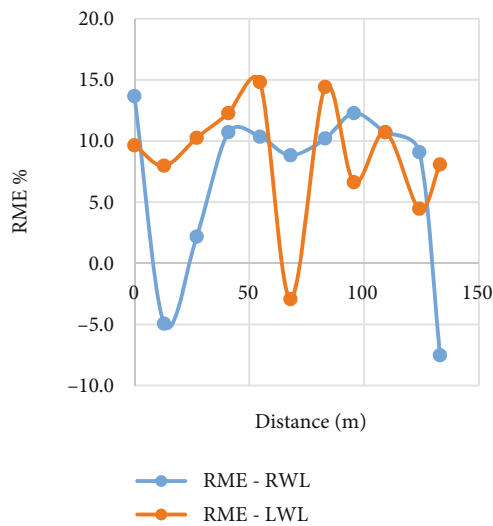


FIGURE 9: Comparison of RME between left and right walls.

These graphs allow giving an estimation of the maximum height at the level of the curved channels.

Table 4 gives the values of the fitting constants α , β , A , B , C for the two laws and the range of applicability.

4.3. Bottom Outlet

4.3.1. Theoretical and Numerical Calculations. The theoretical calculations for the maximum and minimum water level for the bottom outlet were done using equations (9)–(11). The results are shown in Table 6.

In the case of the bottom outlet, we observe from the results of the numerical model (Figure 7) that we have two maximum heights $H_{\max-1}$ and $H_{\max-2}$. The water level near the outer wall is high in comparison to the inner wall, due to the effect of centrifugal force [18]. We can clearly see in the transition zone between the two curved channels the presence of the rooster tail waves, and this generates huge amount of air and turbulence.

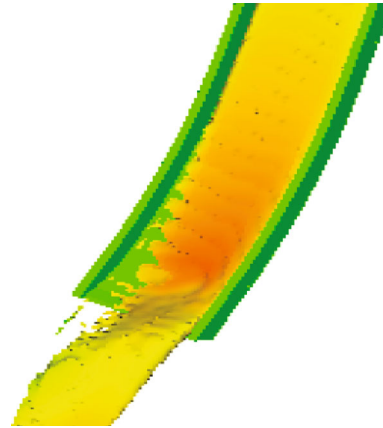


FIGURE 10: The stagnation zone of flow in the ski jump-CFD.

Relative mean error (RME) is given by this formula:

$$\text{RME} = \frac{|\text{Measured value} - \text{computed value}|}{\text{Measured value}} \times 100. \quad (25)$$

The measured value is obtained from the physical model.

The computed value is derived from the CFD calculations.

Table 6 shows that the theoretical maximum height at the level of the first curvature is 3.9 m, whereas a maximum height of 4.39 m was measured for the physical model, which represents a RME of 11.16%. Moreover, for the second curvature a value of 4.3 m was calculated and a corresponding value of 4.71 m was measured, with a RME of 8.7%

4.3.2. Flow Patterns. From Figures 7 and 8, which illustrate the water level, it is clear that we have fluctuations in the bend channel.

In the tests of the physical model, we have noticed an increase in water level in the outer wall in comparison with the inner wall (see Figure 8).

In addition, we observed a zone of disturbance in the intersection of the two curvatures with some water wings. The perturbation due to the first curvature propagates in the direction of the flow and finds a second curvature, which will amplify the effect of this disturbance. Hence, we have high level of water in the physical model as against theoretical calculations and CFD approaches (see Figure 7).

Tables 7 and 8 show the water level in the bottom outlet for the left and right walls for the tested head discharge of the project.

The values in Tables 5 and 6 validate the numerical modelling. The experimental measurements show a good agreement with the values found numerically in terms of the water level, but there are some small deviations that can be explained by the swelling of the water surface due to the interference of the shock waves in the perturbation zone.

For the right part of the wall, the maximum height is 4.35 m and for the left part, the value is 4.48 m.

These results show that we can use the results of the numerical modelling to estimate the height of the walls and optimize them using the physical modelling.

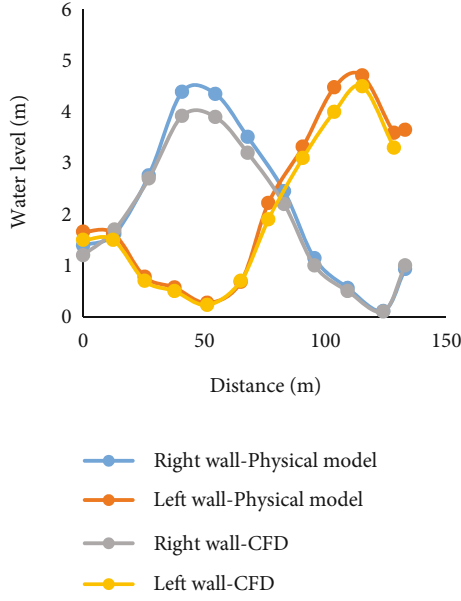


FIGURE 11: Level of water in the bottom outlet.

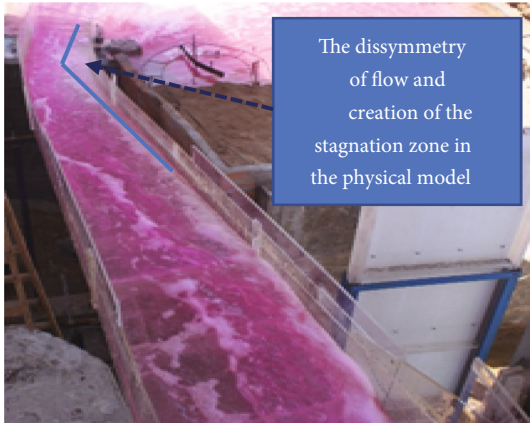
FIGURE 12: Illustration of the dissymmetry of the flow in the chute due to the curvature $R = 400$ m [16].

Figure 9 gives RME for the measured and numerically computed water heights for both walls.

It is noticeable from Figure 9 that the RME does not exceed 15% between the values of the numerical modelling and the experimentation.

This difference can be explained by the huge amount of air generated in this zone, due to the water-air mixing.

The study of the air quantity generated in this critical zone (the intersection of the two curvatures is beyond the scope of this paper).

4.4. Modelling the Spillway without Guide Wall. The curvature in the spillway chute creates a flow dissymmetry at the curvature (see Figure 10).

This phenomenon induces eddies, vortices, and hydraulic jump that will impede the flow and cause erosion of the left wall of spillway chute.

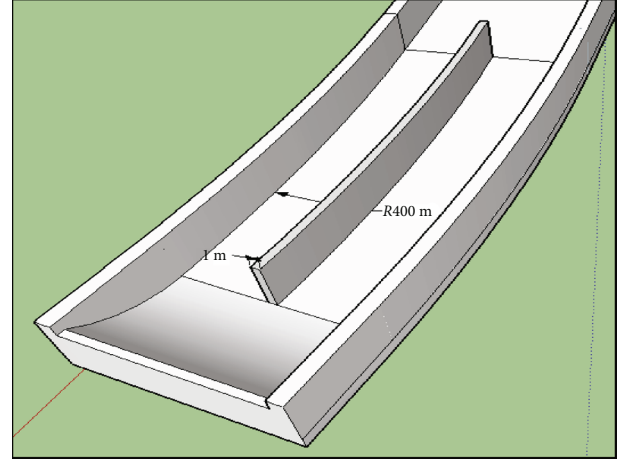


FIGURE 13: Geometry of the guide wall.



FIGURE 14: The stagnation zone of the flow in the ski jump-physical model.

This empty area visible in the ski jump (Figure 10) has been confirmed by the results of the physical model (Figures 12 and 14). This zone of stagnation was created essentially for low head discharges, because the flow doesn't have enough kinetic energy to combat the centrifugal force [18] due to the curvature upstream the ski jump. Therefore, the jet doesn't take off downstream the spillway and generate a vortex (Figure 12).

4.5. Water Surface with Guide Wall. To remedy this phenomenon, and given the great width of the chute, the proposed solution consists of the installation of a separation wall, 1 m thick, with the same height as the inner and outer walls. The dividing wall is located in the middle of the width of the curved chute spillway in order to have an equilibrium distribution of the water surface in this zone (see Figure 13).

After the adding the separating wall, we notice that the results of the numerical and physical modelling present a good agreement with some minimal deviations.

The numerical results can be used to approximately design the sidewalls, while their validation against the experimental data can be used to optimize the height of the walls.

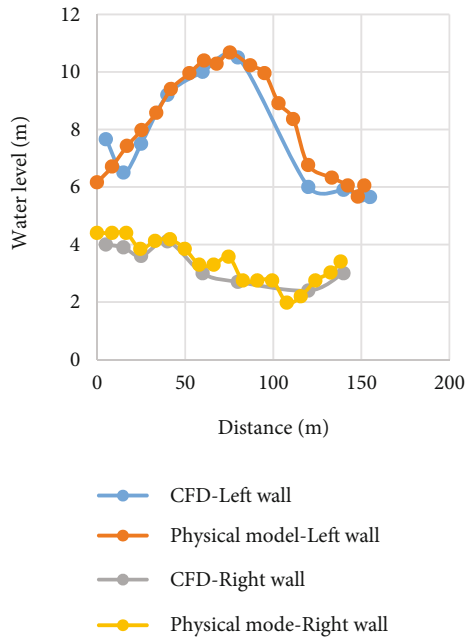


FIGURE 15: Comparison of the water surface for the sidewalls between the experimentation and the numerical methods.

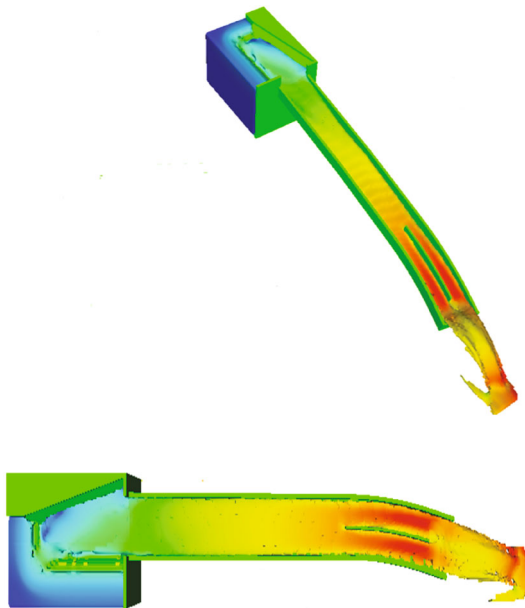


FIGURE 16: Solving numerically the problem of stagnation zone by adding separator wall.

4.6. Modelling the Spillway with Guide Wall. Figure 14 shows the geometry of the separating wall and its size.

The simulation of the spillway with the dividing wall gave a satisfactory result for the resolution of the problem. The flow, shown in Figure 15, became symmetrical to the left and right of the guide wall.

The addition of the guide wall reduced the flow separation in the inner wall and improved the flow behaviour in the chute and the ski jump.



FIGURE 17: The flow in the chute after the addition of the dividing wall-physical model.

Figures 16 and 17 show the validity and efficiency of the proposed solution in terms of the equilibrium of the distribution of the flow over the full width of the chute.

It was also noted that the water jet becomes well distributed over the entire width of the ski jump, which will allow it to take off as far as possible downstream of the dam.

5. Conclusion

In this paper, the flow patterns were investigated using CFD and experimental results, for two case studies: side channel spillway with curved chute and bottom outlet with two curvatures after the gates.

The analysis leads to the following observations and conclusions:

- (i) A 3D numerical model based on RNG $k - \epsilon$ turbulence model was used to study the flow behaviour.
- (ii) Supercritical bend flow contains a plethora of difficulties, shock waves, and vibrations.
- (iii) The numerical approaches and data measured show a fair agreement for the case of curved chute.
- (iv) In the case of bottom outlet, huge amount of air due to the interference of the flow in the perturbation zone.
- (v) The flow without guide wall presents an imbalanced water profile and creates vortex in the ski jump. It is recommended to use this solution for the final design of the spillway to avoid this major problem.
- (vi) The implementation of the dividing wall plays a crucial role in balancing the water surface between the walls; furthermore, the stagnation zone has disappeared, and this allowed flow to have kinetic energy required to take off as far as possible downstream the dam.
- (vii) To the best of authors' knowledge for supercritical bended flow, there is still work to be done to study

the aspects that has not yet acquired attention, for instance, the effect of slope and the shock waves conditions.

Notations

V :	Flow velocity [m/s]
g :	Gravity constant [m/s ²]
h :	Flow depth [m]
ρ :	Water density [kg/m ³]
σ :	Water surface tension [N/m]
ν :	Water kinematic viscosity [m ² /s]
h :	The water height upstream of the curvature [m]
F_0 :	The Froude number of the flow upstream of the curvature
β :	Angle formed by the two wave fronts with the initial direction of flow
θ :	Central angle determined by geometrical considerations
k :	Turbulent kinetic energy [m ² /s ²]
ε :	The turbulent energy dissipation rate
u_i :	Velocity component of x_i [m/s]
μ_{keff}, μ_{eff} :	The effective diffusivity for k , ε , respectively
ν_t :	The turbulent kinetic viscosity [m ² /s]
G :	The production of turbulence due to shear
RME:	Relative mean error
H_{max} :	Maximal height water level in the bottom outlet [m]
H_{min} :	Minimal height water level in the bottom outlet [m]
V_0 :	The approach velocity
ρ_a :	The mean curvature
b :	The width of the channel [m]
R_a :	Radius of curvature [m]
h_e :	The theoretical maximum height [m]
h_0 :	The approach height of water [m]
h_m :	The minimum wave height
h_M :	The maximum wave height
B_0 :	The bend number
θ_m :	The minimum wave angle
θ_M :	The maximum wave angle.

Data Availability

The data availability used to support the finding of this study is included within the article.

Conflicts of Interest

The authors declare that they have no conflicts of interest.

Acknowledgments

This article was funded by Hassania School of Public Works and the Moroccan Hydraulic Laboratory (experimental center of hydraulics).

References

- [1] S. M. Mousavimehr, O. A. Yamini, and M. R. Kavianpour, "Performance assessment of shockwaves of chute spillways in large dams," *Shock and Vibration*, vol. 2021, 2021.
- [2] V. H. Vayghan, M. Mohammadi, and A. Ranjbar, "Experimental study of the rooster tail jump and end sill in horseshoe spillways," *Civil Engineering Journal*, vol. 5, no. 4, pp. 871–880, 2019.
- [3] H. Xue, M. Diao, Q. Ma, and H. Sun, "Hydraulic characteristics and reduction measure for rooster tails behind spillway piers," *Arabian Journal for Science and Engineering*, vol. 43, no. 10, pp. 5597–5604, 2018.
- [4] S. Jung, S. Peetz, and M. Koch, "Poeam—a method for the part orientation evaluation for additive manufacturing," *Sim-A M 2019: II International Conference on Simulation for Additive Manufacturing*, pp. 440–443, 2019.
- [5] A. T. Ippen and R. T. Knapp, "A study of high-velocity flow in curved channels of rectangular cross-section," *Eos, Transactions American Geophysical Union*, vol. 17, no. 2, pp. 516–521, 1936.
- [6] R. Reinauer and W. H. Hager, "Supercritical bend flow," *Journal of Hydraulic Engineering*, vol. 123, no. 3, pp. 208–218, 1997.
- [7] R. Reinauer and W. H. Hager, "Supercritical flow in chute contraction," *Journal of Hydraulic Engineering*, vol. 124, no. 1, pp. 55–64, 1998.
- [8] R. Reinauer and W. H. Hager, "Supercritical flow behind chute piers," *Journal of Hydraulic Engineering*, vol. 120, no. 11, pp. 1292–1308, 1994.
- [9] R. Reinauer and W. H. Hager, "Shockwave in air-water flows," *International Journal of Multiphase Flow*, vol. 22, no. 6, pp. 1255–1263, 1996.
- [10] A. Valiani and V. Caleffi, "Brief analysis of shallow water equations suitability to numerically simulate supercritical flow in sharp bends," *Journal of Hydraulic Engineering*, vol. 131, no. 10, pp. 912–916, 2005.
- [11] M. Ghaeini-Hessaroeyeh, A. Tahershamsi, and M. M. Namin, "Numerical modelling of supercritical flow in rectangular chute bends," *Journal of Hydraulic Research*, vol. 49, no. 5, pp. 685–688, 2011.
- [12] A. Tahershamsi, M. G. Hessaroeyeh, and M. M. Namin, "Two dimensional modeling of dam-break flows," *River Flow*, pp. 555–560, 2010, 2010.
- [13] W. H. Hager, A. J. Schleiss, R. M. Boes, and M. Pfister, *Hydraulic Engineering of Dams*, CRC Press, 2020.
- [14] R. M. Khatsuria, *Hydraulics of Spillways and Energy Dissipators*, CRC Press, 2004.
- [15] R. M. Khatsuria, "Cavitation in spillways and energy dissipators," in *Hydraulics of Spillways and Energy Dissipators*, pp. 541–568, CRC Press, 2004.
- [16] A. C. Quintela, "Flow aeration to prevent cavitation erosion," *International Water Power & Dam Construction United Kingdom*, vol. 32, no. 1, 1980.
- [17] R. P. Regan, A. V. Munch, and E. K. Schader, *Cavitation and erosion damage of sluices and stilling basins at two high-head dams*, in, vol. 50, Proceedings of 13th ICOLD Congress, New Delhi Q, 1979.
- [18] C. Icold, "Selection of design flood," *Bulletin*, vol. 82, Paris, 1992.

- [19] S. Pagliara, S. M. Kurdistani, and T. Roshni, “Rooster tail wave hydraulics of chutes,” *Journal of Hydraulic Engineering*, vol. 137, no. 9, pp. 1085–1088, 2011.
- [20] D. C. Wilcox, *Turbulence Modeling for CFD*, vol. 2, DCW Industries, La Canada, CA, 1998.
- [21] S. Rodriguez, *Applied Computational Fluid Dynamics and Turbulence Modeling*, Springer, 2019.
- [22] B. Blocken and C. Gualtieri, “Ten iterative steps for model development and evaluation applied to Computational Fluid Dynamics for Environmental Fluid Mechanics,” *Environmental Modelling and Software*, vol. 33, pp. 1–22, 2012.
- [23] B. Falck, D. Falck, and B. Collette, *FreeCAD [How-To]*, Packt Publishing Ltd, 2012.